Frontiers of Information Technology & Electronic Engineering
www.jzus.zju.edu.cn; engineering.cae.cn; www.springerlink.com
ISSN 2095-9184 (print); ISSN 2095-9230 (online)
E-mail: jzus@zju.edu.cn

Interval type-2 fuzzy logic based radar task priority assignment method for detecting hypersonic-glide vehicles*

Fanqing MENG‡[1], Kangsheng TIAN[2]

[1]*Department of Graduates, Early Warning Academy, Wuhan 430019, China*

[2]*No. 4 Department, Early Warning Academy, Wuhan 430019, China*

E-mail: maoximengruizhi@126.com; tiankangsheng@sohu.com

Received Oct. 19, 2020; Revision accepted Jan. 18, 2021; Crosschecked Oct. 9, 2021; Published online Feb. 5, 2022

Abstract: A radar task priority assignment method based on interval type-2 fuzzy logic system (IT2FLS) was designed to solve the problem of resource management for phased-array radar to detect hypersonic-glide vehicles (HGVs). The mathematical model of the radar task and the motion and detection models of HGVs are described in detail. The target threat of an HGV is divided into maneuver, speed, azimuth, and distance threats. In the radar task priority assignment method based on IT2FLS, the maneuver factor, speed, azimuth difference, distance, and initial priority are input variables. The radar task priority is the output variable. To reduce the number of fuzzy rules and avoid rule explosion, an IT2FLS with a hierarchical structure was designed. Finally, the feasibility of the task priority assignment method was verified by simulations. Simulation results showed that the method based on IT2FLS has a higher precise tracking rate, mean initial priority, and target threat degree, and a shorter offset time.

Key words: Hypersonic-glide vehicle (HGV); Phased-array radar; Interval type-2 fuzzy logic system (IT2FLS); Priority assignment
https://doi.org/10.1631/FITEE.2000560 **CLC number:** TN958

1 Introduction

The hypersonic-glide vehicle (HGV) is a kind of vehicle that glides at a speed greater than Ma5 at an altitude of 20–100 km. By gliding at hypersonic speed in near space, it has the advantages of high speed and low altitude. There is no evidence to show that traditional ballistic missile defense systems can effectively intercept HGV targets. Therefore, HGV has become a strategic weapon developed by many countries worldwide. In response to the threat of attack from HGVs, ground-based phased-array radar is the main early warning method in addition to early warning satellites. As an electronic scanning radar, phased-array radar has high data rate, high response speed, and the ability to switch between multiple radar tasks without delay. Although phased-array radar can perform a variety of radar tasks, its total resources are limited. Radar resources consumed by radar tasks are different. Therefore, effective management of radar resources is a significant issue to ensure sufficient resource requirements to detect high-value and high-threat targets.

Fig. 1 is a structure diagram of phased-array radar resource management. The dashed box in Fig. 1 is the radar resource manager. The core content of the radar resource manager includes task priority assignment and task scheduling (Jiménez et al., 2012). Different task priorities are assigned to radar tasks to ensure that important tasks have high priority. Task scheduling is based on the principle that high-priority tasks are executed first, and low-priority tasks are executed later. Task priority assignment is an important sub-problem

‡ Corresponding author

* Project supported by the Military Key Project (No. JY2019B137)

ORCID: Fanqing MENG, https://orcid.org/0000-0002-8387-4285

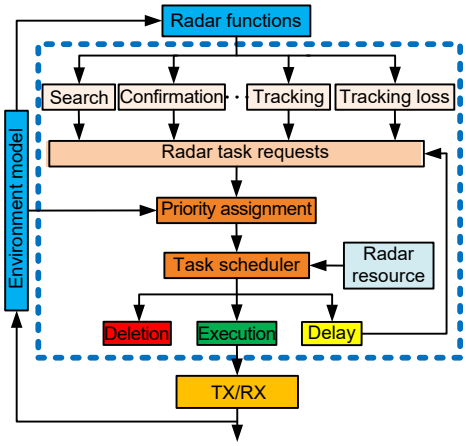

Fig. 1 Radar resource management structure

of radar resource management, related not only to the sequence of task scheduling, but also to the overall resource allocation effect and the operational effectiveness of phased-array radar (Wu et al., 2020). Compared to ordinary aviation targets, HGVs have the characteristics of high speed, low altitude, and maneuverability, which make the battlefield situation more volatile. When detecting HGV targets, if the phased-array radar schedules radar tasks according to a static priority, it cannot adapt to dynamic changes in the battlefield situation. Specifically, in the case of overload, radar resources cannot meet the scheduling requirements of all radar tasks. If the radar task priority does not fully reflect the target threat, it is likely that high-threat targets will be missed due to insufficient radar resources. Therefore, it is necessary to design a radar task priority assignment method that can change in real time to meet the needs of the battlefield situation.

Ding and Moo (2017) used an adaptive multifunctional radar simulation tool to analyze the effectiveness of task priority. By reducing the radar resources assigned to low-priority tasks, more radar resources are available for high-priority tasks. They pointed out that when task priorities are divided, it is necessary to make full use of the kinematic characteristics and attributes of the targets, so as to improve the detection and tracking accuracy of strong and weak maneuvering targets at the small cost of losing low priority target tracking accuracy. To improve the load adaptability of the phased-array radar, a task priority assignment method was designed based on the weighted summation of the initial priority and deadline of the task. The method can be well adapted to the situation of different task loads (Lu et al., 2006). Zhang et al. (2019) designed a radar task scheduling model based on a hybrid adaptive genetic algorithm for the scheduling of phased-array radar. Simulation results showed that the designed model has good performance in terms of global exploration ability, convergence, and robustness. Bao et al. (2018) addressed the issue of radar task priority assignment when passive radar detects radiation sources. Radar task priorities are assigned adaptively according to the threat of radiation sources, which improves the ability to schedule radar tasks corresponding to high threat radiation sources. Aiming at the task priority assignment problem when phased-array radar detects aviation targets and ballistic missile targets (Zhang et al., 2017b, 2017c; Yang et al., 2020), a two-dimensional priority table based assignment method was designed to map the degree of threat and the task deadline to a priority table, jointly determining the priority of radar tasks. Li B et al. (2020) used a dynamic three-way decision method for phased-array radar task scheduling. The target domain was divided into a threat domain, a non-threat domain, and a potential threat domain according to the degree of threat posed by the target. An improved adaptive threshold algorithm was proposed to improve the adaptive capacity of the three-way decision. Miranda et al. (2007) and Guo et al. (2013) designed an adaptive priority assignment method based on fuzzy logic. The method makes full use of the target information sensed by radar or other sensors to assign radar task priorities. Simulation results showed that compared with hard logic and fixed priority assignment methods, the method based on fuzzy logic can change the priority more smoothly. Under high load conditions, the proposed priority assignment method can fully perceive changes in real time in the battlefield environment. It ensures a certain search rate while improving the tracking rate.

The existing radar task priority assignment methods include mainly fixed priority methods, comprehensive priority methods, and fuzzy logic priority methods. The fixed priority assignment method cannot make full use of the target information sensed by radar. It cannot reflect the value or threat of the targets corresponding to different radar tasks (Zhang et al., 2017a, 2018). For the comprehensive priority assignment method, the weighting coefficient of each factor in the

calculation process is manually designated, and the weighting coefficients of the same factor in different studies are not the same. In contrast, the fuzzy logic priority assignment method uses fuzzy reasoning to solve the problem that the weight of each factor cannot be specified accurately in priority assignment, but there is uncertainty in the division of membership functions. When the membership function is finely divided, there is a problem of the explosion of fuzzy rules. For example, the fuzzy logic priority assignment method designed by Miranda et al. (2007) has up to 270 fuzzy rules, which greatly increases the design complexity of the fuzzy system.

Compared with the traditional type-1 fuzzy logic system, the type-2 fuzzy logic system greatly improves the ability to deal with uncertainty (Ontiveros et al., 2020). The type-2 fuzzy logic system can model the uncertainty not only within individuals, but also between them. When realizing the same function, there are fewer rules in a type-2 fuzzy logic system. Because of its excellent characteristics, the type-2 fuzzy logic system has become a focus of new research in the fields of decision-making, control, and machine learning.

Cervantes and Castillo (2015) designed a multivariable control system based on generalized type-2 fuzzy logic integration, and verified the performance of the proposed control system through aircraft flight control problems. Castillo et al. (2016b) compared the efficiency and performance of a generalized type-2 fuzzy logic control approach, interval type-2 fuzzy logic control approach, and type-1 fuzzy logic control approach by four different benchmarks. The experimental results showed that the performance of the generalized type-2 fuzzy logic controller and interval type-2 fuzzy logic controller was obviously better than the counterpart of the type-1 fuzzy logic controller. Castillo et al. (2016a) designed an intelligent controller based on generalized type-2 fuzzy logic, simplified the control problem of complex nonlinear equipment by granular calculation, and verified the performance of the proposed controller using an aircraft control problem. To clarify which type of controller is more suitable for specific applications, Ontiveros-Robles et al. (2018) proposed election criteria for fuzzy logic controllers according to the performance and execution time requirements of the controller. The robustness of a generalized type-2 fuzzy logic controller and an interval type-2 fuzzy logic controller was compared. In the application of medical diagnosis, Ontiveros et al. (2020) compared the performance of a type-1 fuzzy logic system, interval type-2 fuzzy logic system (IT2FLS), and generalized type-2 fuzzy logic system. Simulation results showed that the IT2FLS was the most efficient among these systems.

Moreno et al. (2020) pointed out that the IT2FLS effectively reduces the computational complexity of the type-2 fuzzy logic system. When dealing with problems with a high degree of uncertainty or noise, the advantage of the IT2FLS is obvious. The system effectively improves the ability to deal with uncertainty. The execution time of the system is roughly equivalent to that of the type-1 fuzzy logic system, and significantly lower than that of the type-2 fuzzy logic system (Ontiveros-Robles et al., 2018). Moreover, the system is superior to the type-1 fuzzy logic system in terms of robustness, model-free design, and nonlinear modeling capabilities. Thus, the IT2FLS has been widely used in many fields, such as time-series forecasting, system identification, and control systems. In this study, we design a radar task priority assignment method based on the IT2FLS.

2 Interval type-2 fuzzy logic system

An IT2FLS is composed of a fuzzifier, rule base, inference engine, type reducer, and defuzzifier. The hierarchical structure is shown in Fig. 2 (Mendel, 2017). In Eq. (1), the generalized type-2 fuzzy set is expressed as $\tilde{A}$, and its membership function $\mu_{\tilde{A}}(x, u)$ is a bivariate function on $X\times[0, 1]\rightarrow[0, 1]$, and $0\leqslant\mu_{\tilde{A}}(x, u)\leqslant1$.

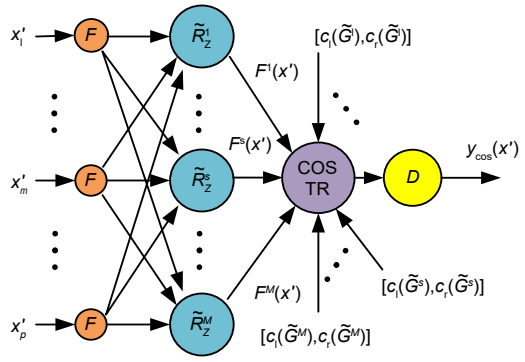

Fig. 2 Hierarchical structure of the interval type-2 fuzzy logic system

X is the universe of the primary variable of $\tilde{A}$, x. U is the universe of the secondary variable u.

$$\tilde{A}=\left\{((x,u),\mu_{\tilde{A}}(x,u))\,|\,x\in X,u\in U\equiv[0,1]\right\}. \quad (1)$$

When $u\in[0, 1]$ and $\mu_{\tilde{A}}(x, u)=1$ for all $x\in X$, the type-2 fuzzy set is called the interval type-2 fuzzy set, which is completely described by its footprint of uncertainty (FOU), and FOU($\tilde{A}$) is shown in Eq. (2):

$$\mathrm{FOU}(\tilde{A})=\{(x,u)|x\in X,u\in[\underline{\mu}_{\tilde{A}}(x),\bar{\mu}_{\tilde{A}}(x)]\}, \quad (2)$$

where $\underline{\mu}_{\tilde{A}}(x)$ and $\bar{\mu}_{\tilde{A}}(x)$ are the lower and upper membership functions (LMF, UMF), respectively (Castillo et al., 2019). In Fig. 3, taking the trapezoidal FOU as an example, the LMF and UMF are shown in Eqs. (3) and (4), respectively.

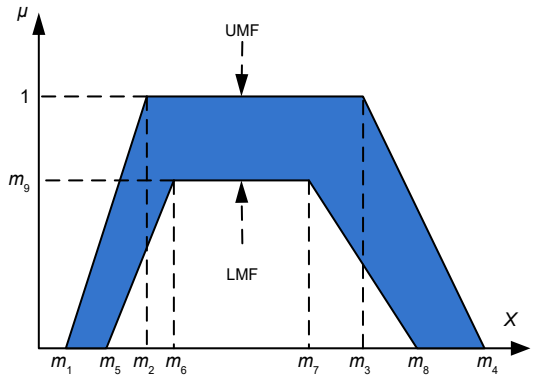

Fig. 3 The FOU of the interval type-2 fuzzy set

$$\underline{\mu}_{\tilde{A}}(x)=\begin{cases}0, & x\leqslant m_1,\\ \dfrac{x-m_1}{m_2-m_1}, & m_1<x\leqslant m_2,\\ 1, & m_2<x\leqslant m_3,\\ \dfrac{m_4-x}{m_4-m_3}, & m_3<x\leqslant m_4,\\ 0, & x>m_4,\end{cases} \quad (3)$$

$$\bar{\mu}_{\tilde{A}}(x)=\begin{cases}0, & x\leqslant m_5,\\ \dfrac{x-m_5}{m_6-m_5}m_9, & m_5<x\leqslant m_6,\\ m_9, & m_6<x\leqslant m_7,\\ \dfrac{m_8-x}{m_8-m_7}m_9, & m_7<x\leqslant m_8,\\ 0, & x>m_8.\end{cases} \quad (4)$$

In Eq. (5), $[\underline{f}^s(x'),\bar{f}^s(x')]$ is the firing interval corresponding to the firing set. The membership function of the s^{th} rule consequent is shown in Eq. (6). From the meet operation of interval type-2 fuzzy sets, Eq. (7) is derived, in which ★ represents the t-norm. Eq. (8) is the FOU of $\tilde{B}^s$.

$$\begin{aligned}F^s(x')&=1\Big/\left[T_{i=1}^{p}\underline{\mu}_{\tilde{F}_i^s}(x_i'),T_{i=1}^{p}\bar{\mu}_{\tilde{F}_i^s}(x_i')\right]\\&=1\Big/\left[\underline{f}^s(x'),\bar{f}^s(x')\right],\end{aligned} \quad (5)$$

$$\mu_{\tilde{G}^s(y)}=1\Big/\left[\underline{\mu}_{\tilde{G}^s}(y),\bar{\mu}_{\tilde{G}^s}(y)\right], \quad (6)$$

$$\mu_{\tilde{B}^s(y|x')}=1\Big/\left[\underline{f}^s(x')\bigstar\underline{\mu}_{\tilde{G}^s}(y),\bar{f}^s(x')\bigstar\bar{\mu}_{\tilde{G}^s}(y)\right], \quad (7)$$

$$\begin{aligned}\mu_{\tilde{B}^s(y|x')}&=1\Big/\left[\underline{\mu}_{\tilde{B}^s}(y|x'),\bar{\mu}_{\tilde{B}^s}(y|x')\right]\\&=1\Big/\mathrm{FOU}(\tilde{B}^s(y|x')).\end{aligned} \quad (8)$$

The center-of-sets (COS) type-reduction method is one of the most widely used methods. As shown in Eq. (9), $Y_{\cos}(x')$ is the set after COS type-reduction. $y_{\mathrm{l}}^{\cos}(x')$ and $y_{\mathrm{r}}^{\cos}(x')$ can be calculated by Eqs. (10) and (11), where L and R are switch points. The values of L and R can be obtained by the enhanced iterative algorithm with the stopping condition algorithm (Mendel, 2017). The output of the defuzzifier is shown in Eq. (12), in which $y_{\cos}(x')$ is the crisp output.

$$Y_{\cos}(x')=\textstyle\sum_{s=1}^{M}w_s\Big/\sum_{s=1}^{M}y_sw_s, \quad (9)$$

where

$$\begin{aligned}&y_s\in\left[c_{\mathrm{l}}(\tilde{G}^s),c_{\mathrm{r}}(\tilde{G}^s)\right],w_s\in\left[\underline{f}^s(x'),\bar{f}^s(x')\right],\\&Y_{\cos}(x')=1\Big/\left[y_{\mathrm{l}}^{\cos}(x'),y_{\mathrm{r}}^{\cos}(x')\right],\end{aligned}$$

$$y_{\mathrm{l}}^{\cos}(x')=\frac{\sum_{s=1}^{L}c_{\mathrm{l}}(\tilde{G}^s)\bar{f}^s(x')+\sum_{s=L+1}^{M}c_{\mathrm{l}}(\tilde{G}^s)\underline{f}^s(x')}{\sum_{s=1}^{L}\bar{f}^s(x')+\sum_{s=L+1}^{M}\underline{f}^s(x')}, \quad (10)$$

$$y_{\mathrm{r}}^{\cos}(x')=\frac{\sum_{s=1}^{R}c_{\mathrm{r}}(\tilde{G}^s)\underline{f}^s(x')+\sum_{s=R+1}^{M}c_{\mathrm{r}}(\tilde{G}^s)\bar{f}^s(x')}{\sum_{s=1}^{R}\underline{f}^s(x')+\sum_{s=R+1}^{M}\bar{f}^s(x')}, \quad (11)$$

$$y_{\cos}(x')=\frac{1}{2}\left[y_{\mathrm{l}}^{\cos}(x')+y_{\mathrm{r}}^{\cos}(x')\right]. \quad (12)$$

3 Mathematical model of the radar task

The radar task model is shown in Eq. (13) (Zhang et al., 2019), in which T_i^k is the k^{th} task in the i^{th} scheduling interval, y_i^k is the task type, p_i^k is the initial priority, c_i^k is the task period, h_i^k is the expected execution time, w_i^k is the time window, d_i^k is the dwell time, e_i^k is the actual execution time, and np_i^k is the number of times the task has been postponed.

$$T_i^k = \left\{ y_i^k, p_i^k, c_i^k, h_i^k, w_i^k, d_i^k, e_i^k, \mathrm{np}_i^k \right\}. \tag{13}$$

The conversion diagram of radar tasks is shown in Fig. 4. The radar first generates a series of search tasks to search the designated airspace. When the target echo is found, a confirmation task is generated to confirm the target. If the confirmation is successful, a periodic tracking task will be generated; otherwise, the search task will continue to be generated. If the target is found to be lost in the process of tracking, a tracking loss task is generated. If the target is reacquired, a periodic tracking task will be generated; otherwise, the reacquisition fails and a search task is generated.

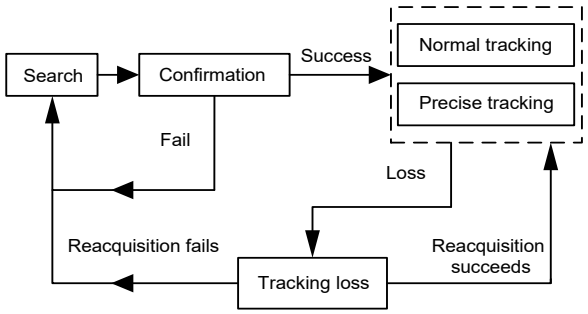

Fig. 4 Radar tasks conversion diagram

4 Radar task priority assignment

4.1 Hypersonic-glide vehicle model

4.1.1 Hypersonic-glide vehicle motion model

As shown in Fig. 5, the motion model is established according to the force of the HGV in the glide phase (Kumar et al., 2018). In Eq. (14), V is the flight speed, γ is the flight path angle, χ is the velocity heading angle, (x, y, z) is the vehicle position in the ground coordinate system, m is the vehicle mass, g_0 is the gravity acceleration, L is the lift, and D is the drag (Li GH et al., 2015).

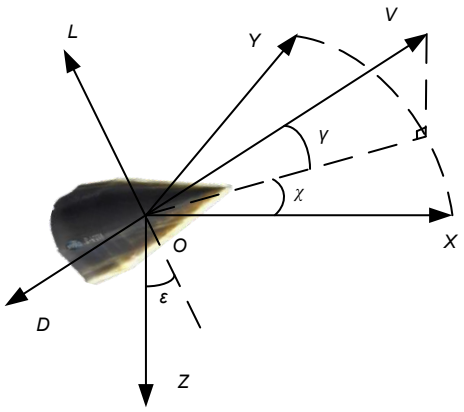

Fig. 5 Motion model of the hypersonic-glide vehicle

$$\begin{cases} \dot{V} = -\dfrac{D}{m} - g_0 \sin\gamma, \\ \dot{\gamma} = \dfrac{L\cos\varepsilon}{mV} - \dfrac{g_0\cos\gamma}{V}, \\ \dot{\chi} = \dfrac{L\sin\varepsilon}{mV\cos\gamma}, \\ \dot{x} = V\cos\gamma\cos\chi, \\ \dot{y} = V\cos\gamma\sin\chi, \\ \dot{z} = -V\sin\gamma. \end{cases} \tag{14}$$

4.1.2 Hypersonic-glide vehicle detection model

The probability of detecting the target can be calculated by Eq. (15), in which V_{T} is the detection threshold and n_{p} is the number of accumulated pulses.

$$P_{\mathrm{D}} = \begin{cases} \exp\left(\dfrac{-V_{\mathrm{T}}}{1+n_{\mathrm{p}}\mathrm{SNR}/2}\right)\left(1+\dfrac{2}{n_{\mathrm{p}}\mathrm{SNR}}\right)^{n_{\mathrm{p}}-2} \\ \cdot\left[1+\dfrac{V_{\mathrm{T}}}{1+n_{\mathrm{p}}\mathrm{SNR}/2}-\dfrac{2(n_{\mathrm{p}}-2)}{n_{\mathrm{p}}\mathrm{SNR}}\right], n_{\mathrm{p}}=1,2, \\ \dfrac{V_{\mathrm{T}}{}^{n_{\mathrm{p}}-1}\mathrm{e}^{-V_{\mathrm{T}}}}{(1+n_{\mathrm{p}}\mathrm{SNR}/2)(n_{\mathrm{p}}-2)!}+1-\Gamma_{\mathrm{I}}(V_{\mathrm{T}},n_{\mathrm{p}}-1) \\ +\left[1+\dfrac{V_{\mathrm{T}}}{1+n_{\mathrm{p}}\mathrm{SNR}/2}-\dfrac{2(n_{\mathrm{p}}-2)}{n_{\mathrm{p}}\mathrm{SNR}}\right] \\ \cdot\Gamma_{\mathrm{I}}\left(\dfrac{V_{\mathrm{T}}}{1+2/(n_{\mathrm{p}}\mathrm{SNR})},n_{\mathrm{p}}-1\right), n_{\mathrm{p}}>2, \end{cases} \tag{15}$$

In Eq. (16), the signal-to-noise ratio (SNR) of target detection can be obtained from the radar equation (Xiao et al., 2015). SNR_o is the radar receiver output SNR, P_t is the radar peak power, G is the radar antenna gain, λ is the radar signal wavelength, σ is the radar cross section (RCS) of the target, K is the Boltzmann constant, T_e is the effective noise temperature, B is the radar signal bandwidth, F is the noise coefficient, L is the radar loss, and R is the distance between the target and the radar.

$$\mathrm{SNR}_o = \frac{P_t G^2 \lambda^2 \sigma}{(4\pi)^3 K T_e B F L R^4}. \tag{16}$$

4.2 Target threat

4.2.1 Maneuver threat

An HGV in near space can maneuver in the longitudinal and lateral planes to enhance survivability. According to Meng et al. (2020), the typical trajectories of HGVs in near space can be divided into a longitudinal equilibrium glide trajectory, longitudinal skip glide trajectory, lateral no maneuver trajectory, lateral weak maneuver trajectory, and lateral strong maneuver trajectory. The maneuvering threat $T_d(M)$ can be determined by experts according to ballistic trajectories.

4.2.2 Speed threat

The greater the flight speed, the greater the speed threat. A standard 0–1 transformation is used to process the vehicle speed in a dimensionless manner. The speed threat function $T_d(V)$ is shown in Eq. (17), where $V_{\min}$ and $V_{\max}$ are the two boundary values of the flight speed.

$$T_d(V) = \begin{cases} 0, & V < V_{\min}, \\ \dfrac{V - V_{\min}}{V_{\max} - V_{\min}}, & V_{\min} \leqslant V \leqslant V_{\max}, \\ 1, & V_{\max} < V. \end{cases} \tag{17}$$

4.2.3 Azimuth threat

The azimuth difference between the vehicle and the radar is shown in Eq. (18). When the velocity heading angle is on the left side of the vehicle-radar line of sight, it is positive. (x_r, y_r, z_r) is the radar position. When the vehicle flies toward the radar, the azimuth threat is great; when it flies away from the radar, the azimuth threat is small. The azimuth threat function $T_d(\Delta\chi)$ is shown in Eq. (19), where $\Delta\chi_{\min}$ and $\Delta\chi_{\max}$ are the two boundary values of the azimuth difference.

$$\Delta\chi = \begin{cases} \dfrac{y_r - y}{|y_r - y|} \arccos\left[\dfrac{x_r - x}{\sqrt{(x_r - x)^2 + (y_r - y)^2}}\right] - \chi, & \\ & y_r - y \neq 0, \\ \chi, & y_r - y = 0, \end{cases} \tag{18}$$

$$T_d(\Delta\chi) = \frac{|\Delta\chi_{\max}| - |\Delta\chi|}{|\Delta\chi_{\max}| - |\Delta\chi_{\min}|}. \tag{19}$$

4.2.4 Distance threat

The distance threat function $T_d(R)$ is shown in Eq. (20). R is the distance between the vehicle and the radar. $R_{\min}$ and $R_{\max}$ are the two boundary values of the distance. $R_{\min}$ is determined by the combat radius of the terminal air defense interceptor weapon. $R_{\max}$ is determined by the radar's maximum visual range to the HGV in near space.

$$T_d(R) = \begin{cases} 1, & R < R_{\min}, \\ \dfrac{R_{\max} - R}{R_{\max} - R_{\min}}, & R_{\min} \leqslant R \leqslant R_{\max}, \\ 0, & R_{\max} < R. \end{cases} \tag{20}$$

4.3 Task priority

4.3.1 IT2FLS with a hierarchical structure

Fig. 6 is a decision tree of radar task priority assignment. Wang (1999) pointed out that a fuzzy logic system with a hierarchical structure can effectively reduce the number of fuzzy rules. Assume that a fuzzy logic system has n input variables, and that each input variable has m fuzzy values. When the hierarchical structure is not adopted, the number of fuzzy rules is m^n. When using a hierarchical structure, the number of fuzzy rules is $(n-1)m^2$. The number of fuzzy rules changes from an exponential function of the input variable to a linear function of the input

variable, so that the rule explosion problem can be effectively solved.

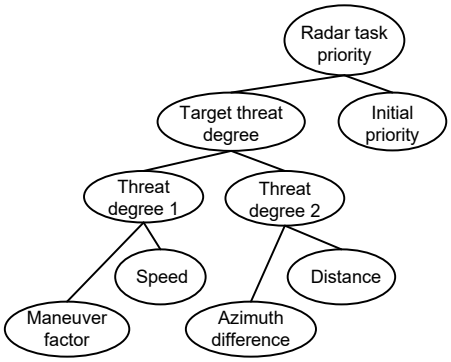

Fig. 6 Decision tree of priority assignment

Fig. 7 shows the number of fuzzy rules with different structures. When the fuzzy logic system has five input variables and each input variable has three fuzzy values, compared with a fuzzy logic system without a hierarchical structure, the use of the fuzzy logic system designed in this study reduces the number of fuzzy rules by 207 (about 85.2%). When the fuzzy logic system has five input variables and each input variable has five fuzzy values, compared with a fuzzy logic system without a hierarchical structure, the use of the fuzzy logic system designed here reduces the number of fuzzy rules by 3025 (about 96.8%).

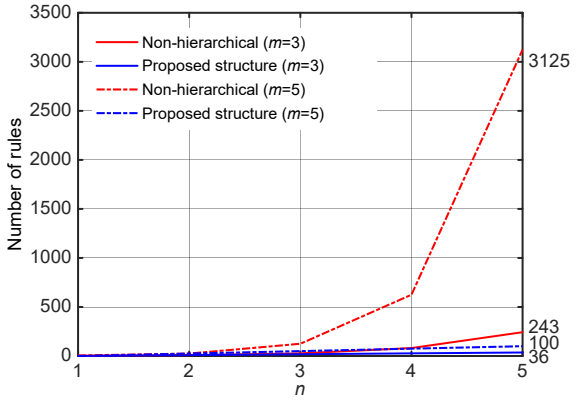

Fig. 7 Number of fuzzy rules

4.3.2 IT2FLS of radar task priority

Take a fuzzy subsystem composed of target threat degree, initial priority, and radar task priority as an example. The target threat degree and initial priority are the inputs of the fuzzy subsystem and the radar task priority is the output. Table 1 shows the fuzzy variables and fuzzy values of the fuzzy subsystem. The target threat degree is the input x_1, the initial priority is the input x_2, and the radar task priority is the output y. The fuzzy values of x_1 are $\tilde{X}_{11}$, $\tilde{X}_{12}$, and $\tilde{X}_{13}$. The fuzzy values of x_2 are $\tilde{X}_{21}$, $\tilde{X}_{22}$, and $\tilde{X}_{23}$. The fuzzy values of y are $\tilde{G}^1$, $\tilde{G}^2$, $\tilde{G}^3$, $\tilde{G}^4$, and $\tilde{G}^5$. The rule base is shown in Table 2. As shown in Fig. 8, the FOUs of $\tilde{X}_{11}$, $\tilde{X}_{12}$, and $\tilde{X}_{13}$ are represented by nine-point vectors, which are (0.0, 0.0, 0.2, 0.5, 0.0, 0.0, 0.0, 0.3, 1.0), (0.2, 0.4, 0.6, 0.8, 0.3, 0.5, 0.5, 0.7, 1.0), and (0.5, 0.8, 1.0, 1.0, 0.7, 1.0, 1.0, 1.0, 1.0). As shown in Fig. 9, the FOUs of $\tilde{X}_{21}$, $\tilde{X}_{22}$, and $\tilde{X}_{23}$ are represented by nine-point vectors: (0.0, 0.0, 1.0, 2.5, 0.0, 0.0, 0.0, 1.5, 1.0), (1.0, 2.0, 3.0, 4.0, 1.5, 2.5, 2.5, 3.5, 1.0), and (2.5, 4.0, 5.0, 5.0, 3.5, 5.0, 5.0, 5.0, 1.0). The membership functions of consequents of rules are $\mu_{\tilde{G}^1(y)} = 1/[0, 0.2]$, $\mu_{\tilde{G}^2(y)} = 1/[0.2, 0.4]$, $\mu_{\tilde{G}^3(y)} = 1/[0.4, 0.6]$, $\mu_{\tilde{G}^4(y)} = 1/[0.6, 0.8]$, and $\mu_{\tilde{G}^5(y)} = 1/[0.8, 1]$. Fig. 10 is the crisp output of radar task priority.

5 Simulation verification and analysis

5.1 Experiment parameter settings

To verify the performance of the proposed priority assignment method, the following experiments were designed. The priority assignment methods of Lu et al. (2006) and Guo et al. (2013) were selected and marked as method 1 and method 2, respectively, for comparison with our proposed method. The simulation parameters were set as follows: Taking the hypersonic common aero vehicle (CAV-H) as an example (Duan et al., 2010), 100 batches of targets with random initial speeds and initial positions were generated (Li GH et al.,

Table 1 Fuzzy variables and fuzzy values

Fuzzy variable	Fuzzy value
Target threat degree (x_1)	$\tilde{X}_{11}$(weak), $\tilde{X}_{12}$(medium), $\tilde{X}_{13}$(strong)
Initial priority (x_2)	$\tilde{X}_{21}$(low), $\tilde{X}_{22}$(medium), $\tilde{X}_{23}$(high)
Radar task priority (y)	$\tilde{G}^1$(low), $\tilde{G}^2$(medium-low), $\tilde{G}^3$(medium), $\tilde{G}^4$(medium-high), $\tilde{G}^5$(high)

Table 2 Fuzzy rule base

Rule No.	IF		THEN
	x_1	x_2	y
$\tilde{R}_Z^1$	$\tilde{X}_{11}$	$\tilde{X}_{21}$	$\tilde{G}^1$
$\tilde{R}_Z^2$	$\tilde{X}_{11}$	$\tilde{X}_{22}$	$\tilde{G}^2$
$\tilde{R}_Z^3$	$\tilde{X}_{11}$	$\tilde{X}_{23}$	$\tilde{G}^3$
$\tilde{R}_Z^4$	$\tilde{X}_{12}$	$\tilde{X}_{21}$	$\tilde{G}^2$
$\tilde{R}_Z^5$	$\tilde{X}_{12}$	$\tilde{X}_{22}$	$\tilde{G}^3$
$\tilde{R}_Z^6$	$\tilde{X}_{12}$	$\tilde{X}_{23}$	$\tilde{G}^4$
$\tilde{R}_Z^7$	$\tilde{X}_{13}$	$\tilde{X}_{21}$	$\tilde{G}^3$
$\tilde{R}_Z^8$	$\tilde{X}_{13}$	$\tilde{X}_{22}$	$\tilde{G}^4$
$\tilde{R}_Z^9$	$\tilde{X}_{13}$	$\tilde{X}_{23}$	$\tilde{G}^5$

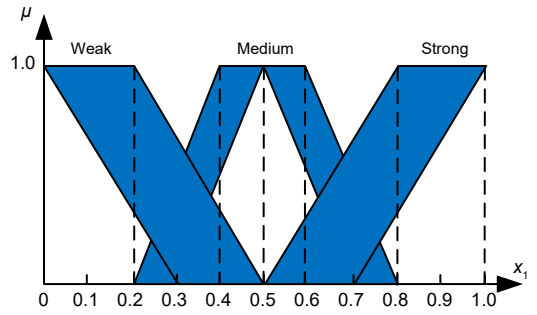

Fig. 8 The FOU of the fuzzy value for target threat degree

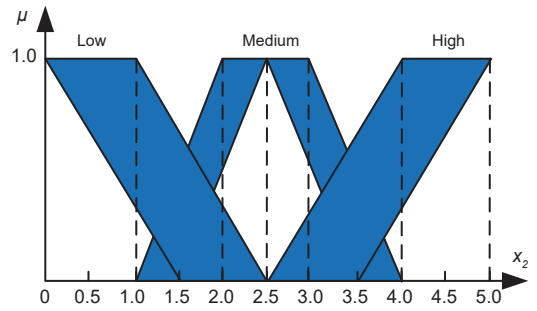

Fig. 9 The FOU of the fuzzy value for initial priority

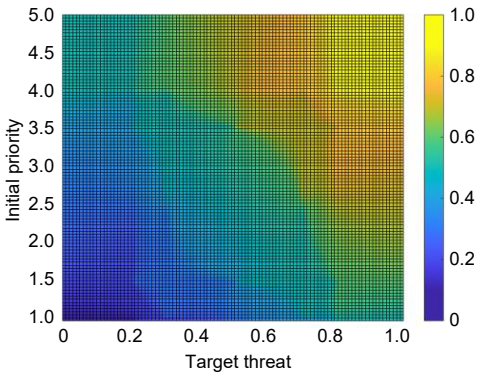

Fig. 10 The crisp output of radar task priority

2017). The radar position was (1500, 0, –0.1) km, the radar operating frequency was f_r=433 MHz, the transmit and receive gain was G=41 dB, the radar transmit peak power was P_t=1164 kW, and the radar duty cycle was 25%. The RCS of the target was RCS= 0.1 m^2, the target detection probability was P_d=0.9, and the false alarm rate was P_{fa}=1×10^{-6}.

The trajectories of the partial targets are shown in Fig. 11. Fig. 12 shows the flight speeds of the HGVs. Fig. 13 shows the azimuth difference between the HGVs and the radar. Fig. 14 shows the distance between the HGVs and the radar.

Table 3 shows the initial priority, dwell time, time window, and period of the radar tasks. The length of the scheduling interval was SI$_i$=50 ms, and the total number of scheduling intervals was M=200. V_{max}= 7900 m/s, V_{min}=1700 m/s, R_{max}=1200 km, R_{min}=200 km, $\Delta\chi_{max}$=180°, $\Delta\chi_{min}$=−180°. Figs. 15 and 16 show the

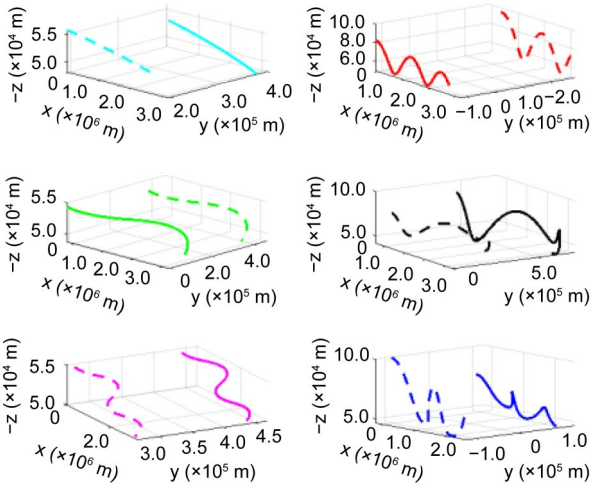

Fig. 11 The ballistic trajectories of the HGVs

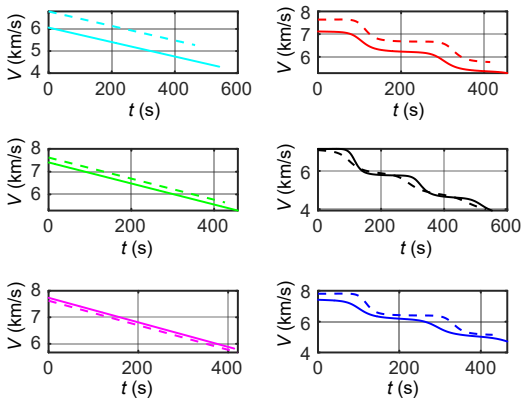

Fig. 12 The flight speeds of the HGVs

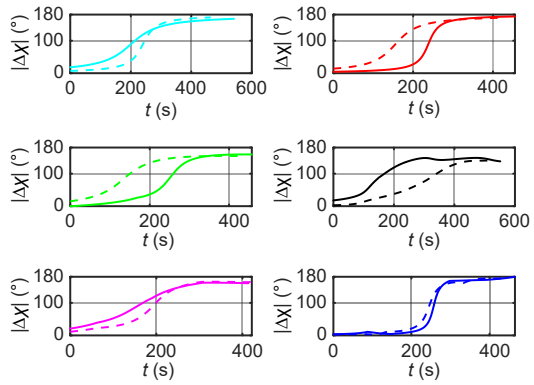

Fig. 13 The azimuth difference between the HGVs and the radar

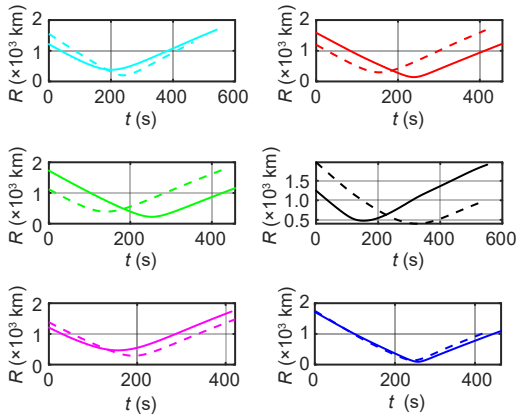

Fig. 14 The distance between the HGVs and the radar

Table 3 Radar task parameters

Task type	Initial priority	Dwell time (ms)	Time window (ms)	Task cycle (ms)
Confirmation	5	7	30	–
Precise tracking	4	5	30	500
Tracking loss	3	7	40	–
Normal tracking	2	8	50	1000
Search	1	9	100	2000

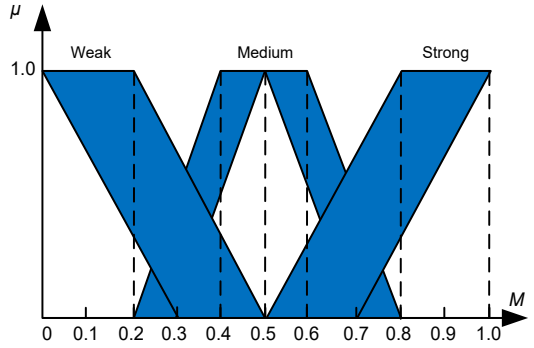

Fig. 15 The FOU of the fuzzy value for the maneuver factor

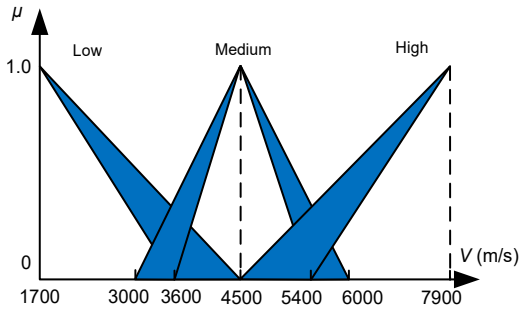

Fig. 16 The FOU of the fuzzy value for speed

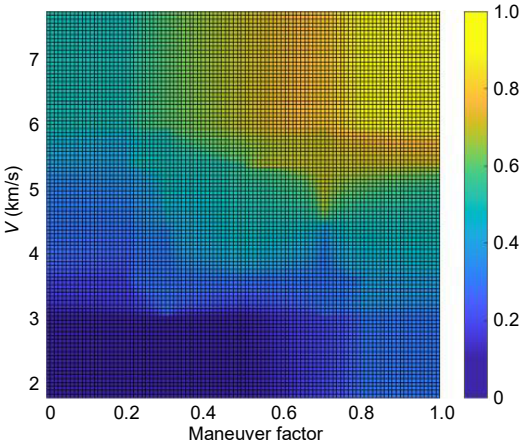

Fig. 17 The crisp output of threat degree 1

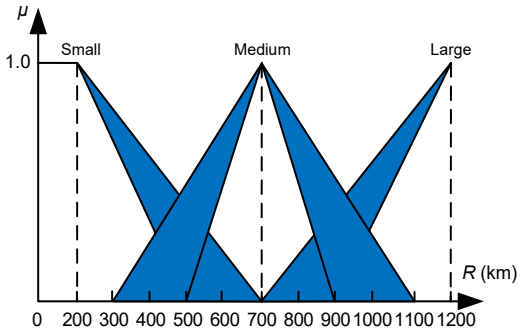

Fig. 18 The FOU of the fuzzy value for distance

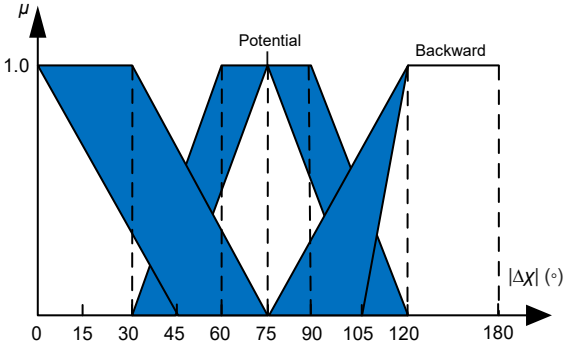

Fig. 19 The FOU of the fuzzy value for azimuth difference

FOUs of the fuzzy values for the maneuver factor and flight speed, respectively. Fig. 17 shows the crisp output of threat degree 1. Figs. 18 and 19 show the FOUs of the fuzzy values for the distance and the azimuth difference between the HGV and the radar, respectively. Fig. 20 shows the crisp output of threat degree 2.

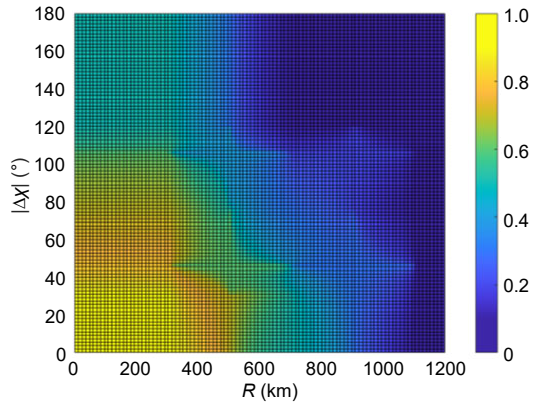

Fig. 20 The crisp output of threat degree 2

5.2 Analysis of experimental results

Fig. 21 shows the length of the remaining time slices in each scheduling interval of the three methods under the condition of 96 batches of targets. The remaining time slices were all less than 2.8 ms, and it was no longer possible to schedule more radar tasks in each scheduling interval. The three methods made full use of the time resources of each scheduling interval.

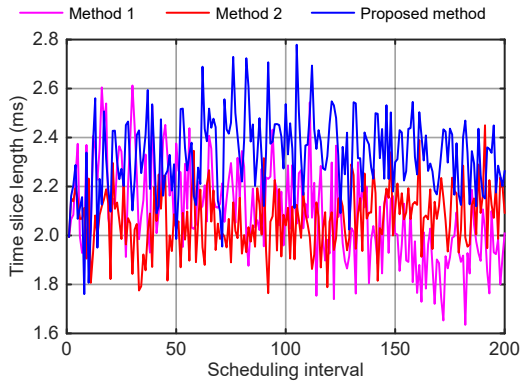

Fig. 21 The length of the remaining time slices in each scheduling interval

References to color refer to the online version of this figure

Fig. 22 shows part of the task scheduling results of the three methods under the condition of 96 batches of targets. When radar task priority assignment was carried out using our proposed method, the number of high initial priority tasks successfully scheduled was obviously greater than those scheduled by methods 1 and 2.

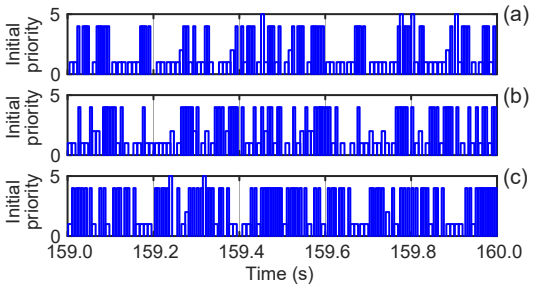

Fig. 22 The task scheduling results of method 1 (a), method 2 (b), and our proposed method (c)

5.2.1 Initial priority

Fig. 23 shows the mean initial priority of radar tasks in the execution queue. As the number of targets increased, the mean initial priority of the radar tasks in the execution queue of the three methods showed an increasing trend. When the radar task priority was assigned by our proposed method, the mean initial priority of the radar task in the execution queue was the highest. When there were more than 50 batches of targets, the mean initial priority of our proposed method was about 21.3% higher than that of method 1, and about 16.5% higher than that of method 2.

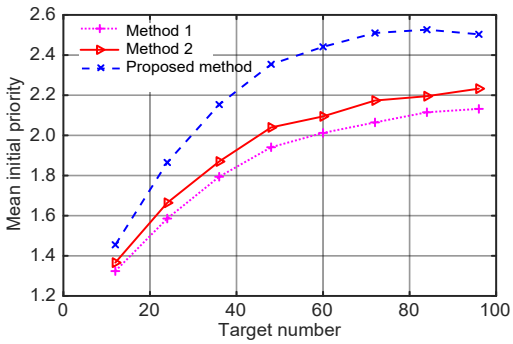

Fig. 23 The mean initial priority of radar tasks in the execution queue

Fig. 24 shows the mean initial priority of radar tasks in the deleted queue. With the increase in the

number of targets, the mean initial priority of the radar tasks in the deleted queue showed an increasing trend. When using our proposed method to assign the radar task priorities, the mean initial priority of the radar task in the deleted queue was the lowest. When there were more than 70 batches of targets, the mean initial priority of radar tasks in the deleted queue of our proposed method was significantly lower than that of methods 1 and 2.

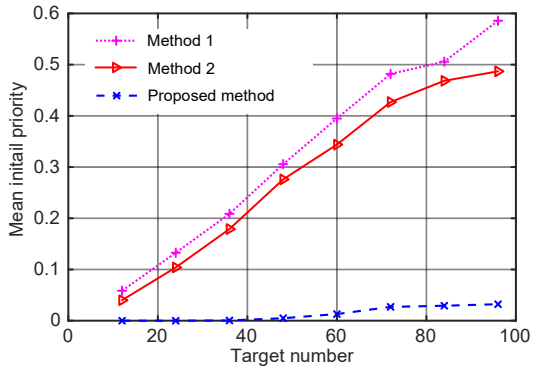

Fig. 24 The mean initial priority of radar tasks in the deleted queue

5.2.2 Target threat degree

Fig. 25 shows the maneuver threat of radar tasks in the execution queue. As the number of targets increased, the maneuver threat of the three methods also increased. When the radar task priority was assigned by our proposed method, the radar tasks had the greatest maneuver threat. When there were more than 50 batches of targets, the maneuver threat of our proposed method was about 40.3% higher than that of method 1, and 28.8% higher than that of method 2.

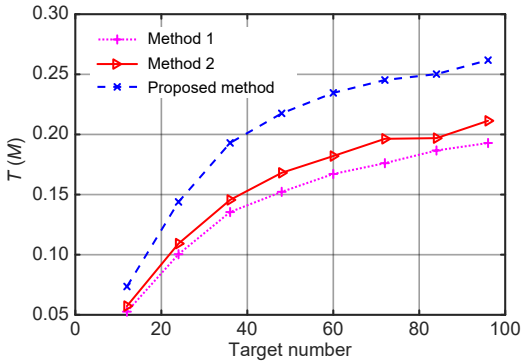

Fig. 25 Maneuver threat of the radar tasks

Fig. 26 shows the speed threat of radar tasks in the execution queue. As the number of targets increased, the speed threat of the three methods all showed an upward trend. When the radar task priority was assigned by our proposed method, the speed threat of the radar tasks was the highest. When there were more than 50 batches of targets, the speed threat of our proposed method was about 39.6% higher than that of method 1, and 27.4% higher than that of method 2.

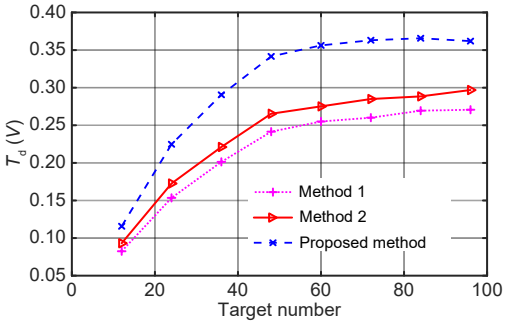

Fig. 26 Speed threat of the radar tasks

Fig. 27 shows the azimuth threat of radar tasks in the execution queue. As the number of targets increased, the azimuth threat of the three methods all showed an upward trend. When the radar task priority was assigned by our proposed method, the azimuth threat of the radar task was the highest. When there were more than 50 batches of targets, the azimuth threat of our proposed method was about 38.2% higher than that of method 1, and 26.1% higher than that of method 2.

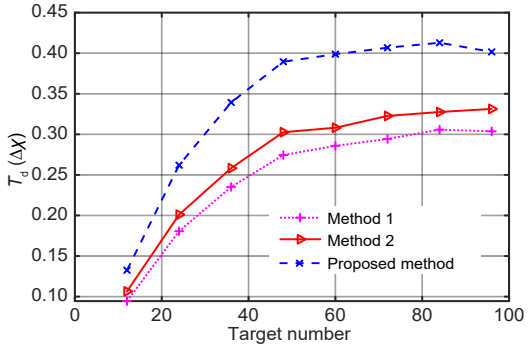

Fig. 27 Azimuth threat of the radar tasks

Fig. 28 shows the distance threat of radar tasks in the execution queue. As the number of targets

increased, the distance threat of the three methods all showed an upward trend. When using our proposed method to assign the priority of radar tasks, the distance threat of radar tasks was the highest. When there were more than 50 batches of targets, the distance threat of our proposed method was about 42.3% higher than that of method 1, and 30.2% higher than that of method 2.

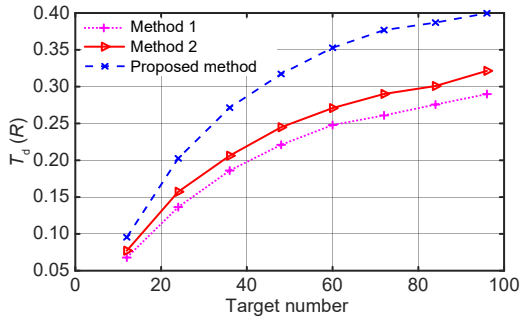

Fig. 28 Distance threat of the radar tasks

5.2.3 Search rate and precise tracking rate

Fig. 29 shows the search rate of the radar tasks. As the number of targets increased, the radar task search rates of the three methods all showed a downward trend. When the radar task priority was assigned by our proposed method, the search rate was the lowest. When the targets were fewer than 48 batches, the search rates of the three methods were all higher than 0.5. When the targets were greater than 60 batches, the search rate of our proposed method dropped to below 0.5, about 14.3% lower than that of method 1, and about 11.1% lower than that of method 2.

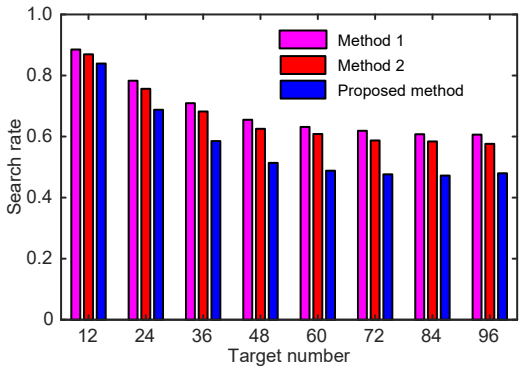

Fig. 29 Search rate of the radar tasks

Fig. 30 shows the precise tracking rate of the radar tasks. As the number of targets increased, the precise tracking rates of the three methods showed an upward trend. When the radar task priority was assigned by our proposed method, the precise tracking rate of the radar tasks was the highest. When the targets were fewer than 36 batches, the precise tracking rates of the three methods were less than 0.4. When the targets were larger than 48 batches, the precise tracking rate of our proposed method increased to more than 0.4, about 14.8% higher than that of of method 1, and about 10.8% higher than that of method 2.

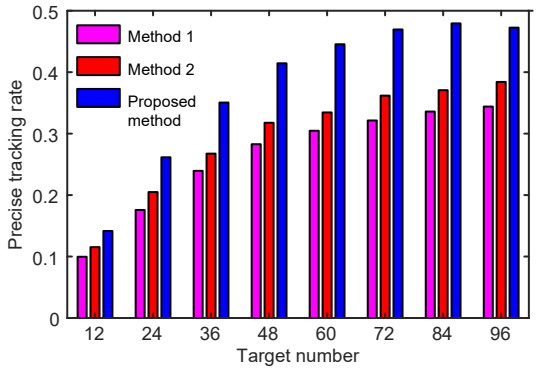

Fig. 30 Precise tracking rate of the radar tasks

5.2.4 Offset time and scheduling success rate

Fig. 31 shows the offset between the actual and expected execution time of the radar tasks. As the number of targets gradually increased, the offset time of the three methods all showed a downward trend. As the number of targets increased, the number of precise tracking radar tasks increased accordingly. The dwell time and time window of precise tracking tasks were the shortest among all radar tasks, so the offset time of radar tasks showed a gradual decline. When the targets were greater than 60 batches, the offset time of our proposed method was about 22.8% lower than that of method 1, and about 10.5% lower than that of method 2.

Fig. 32 shows the scheduling success rate of radar tasks. The scheduling success rates of the three methods did not show a significant upward or downward trend with the increase in the number of incoming targets, and remained stable in the range of 0.83–0.85.

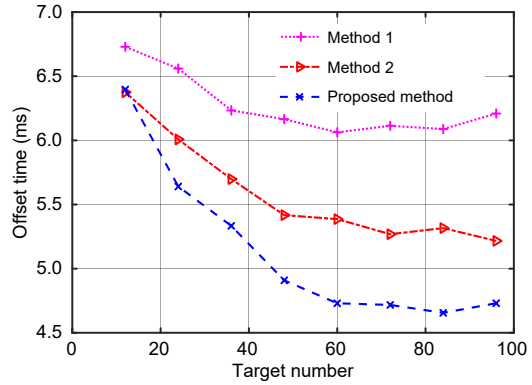

Fig. 31 Offset time of the radar tasks

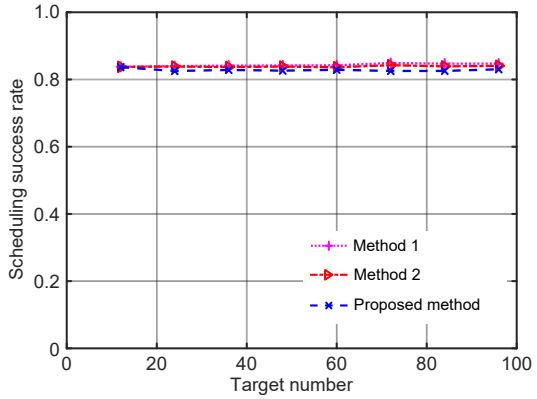

Fig. 32 Scheduling success rate of the radar tasks

6 Conclusions

In this research we designed a task priority assignment method based on IT2FLS with the aim of alleviating the radar resource management problem when ground-based phased-array radar detects HGVs in near space. Compared with the methods proposed by Lu et al. (2006) and Guo et al. (2013), the method proposed in this study has stronger information perception ability and can effectively screen radar tasks with high threat and high initial priority. When the targets were greater than 50 batches, the mean initial priority, target threat degree, and precise tracking rate of our proposed method were significantly higher. While maintaining an equivalent scheduling success rate, the task offset time of our proposed method was significantly lower.

In future work, it is necessary to study the robustness of IT2FLS and analyze the influence of the FOU of the fuzzy value on the performance of IT2FLS. It will also be necessary to analyze the influence of the number of fuzzy rules on the performance of IT2FLS, and to study how to reduce the number of fuzzy rules while ensuring that the system performance does not decrease, thereby reducing the complexity of system design.

Contributors

Fanqing MENG designed the research, processed the data, and drafted the paper. Kangsheng TIAN revised and finalized the paper.

Compliance with ethics guidelines

Fanqing MENG and Kangsheng TIAN declare that they have no conflict of interest.

References

Bao PF, Huang XP, Zhou XC, 2018. Adaptive scheduling algorithm for passive radar tasks with integrated priority. *Mod Def Technol*, 46(1):141-147, 183 (in Chinese). https://doi.org/10.3969/j.issn.1009-086x.2018.01.023

Castillo O, Cervantes L, Soria J, et al., 2016a. A generalized type-2 fuzzy granular approach with applications to aerospace. *Inform Sci*, 354:165-177. https://doi.org/10.1016/j.ins.2016.03.001

Castillo O, Amador-Angulo L, Castro JR, et al., 2016b. A comparative study of type-1 fuzzy logic systems, interval type-2 fuzzy logic systems and generalized type-2 fuzzy logic systems in control problems. *Inform Sci*, 354:257-274. https://doi.org/10.1016/j.ins.2016.03.026

Castillo O, Melin P, Ontiveros E, et al., 2019. A high-speed interval type 2 fuzzy system approach for dynamic parameter adaptation in metaheuristics. *Eng Appl Artif Intell*, 85:666-680. https://doi.org/10.1016/j.engappai.2019.07.020

Cervantes L, Castillo O, 2015. Type-2 fuzzy logic aggregation of multiple fuzzy controllers for airplane flight control. *Inform Sci*, 324:247-256. https://doi.org/10.1016/j.ins.2015.06.047

Ding Z, Moo P, 2017. Benefits of target prioritization for phased array radar resource management. Proc 18th Int Radar Symp, p.1-7. https://doi.org/10.23919/IRS.2017.8008153

Duan GR, Sun Y, Zhang MR, et al., 2010. Aerodynamic coefficients models of hypersonic vehicle based on aero database. Proc 1st Int Conf on Pervasive Computing, Signal Processing and Applications, p.1001-1004. https://doi.org/10.1109/PCSPA.2010.247

Guo KP, Zuo Y, Xue AK, 2013. An adaptive task scheduling algorithm based on the fuzzy logic priority for multifunction radars. *J Jiangnan Univ (Nat Sci Ed)*, 12(5):591-595 (in Chinese). https://doi.org/10.3969/j.issn.1671-7147.2013.05.015

Jiménez MI, del Val L, Villacorta JJ, et al., 2012. Design of task scheduling process for a multifunction radar. *IET Radar Sonar Navig*, 6(5):341-347.

https://doi.org/10.1049/iet-rsn.2011.0309

Kumar GN, Ikram M, Sarkar AK, et al., 2018. Hypersonic flight vehicle trajectory optimization using pattern search algorithm. *Optim Eng*, 19(1):125-161. https://doi.org/10.1007/s11081-017-9367-0

Li B, Tian LY, Chen DQ, et al., 2020. A task scheduling algorithm for phased-array radar based on dynamic three-way decision. *Sensors*, 20(1):153. https://doi.org/10.3390/s20010153

Li GH, Zhang HB, Tang GJ, 2015. Maneuver characteristics analysis for hypersonic glide vehicles. *Aerosp Sci Technol*, 43:321-328. https://doi.org/10.1016/j.ast.2015.03.016

Li GH, Zhang HB, Tang GJ, 2017. Flight-corridor analysis for hypersonic glide vehicles. *J Aerosp Eng*, 30(1):06016005. https://doi.org/10.1061/(ASCE)AS.1943-5525.0000667

Lu JB, Hu WD, Yu WX, 2006. Study on real-time task scheduling of multifunction phased array radars. *Acta Electron Sin*, 34(4):732-736 (in Chinese). https://doi.org/10.3321/j.issn:0372-2112.2006.04.032

Mendel JM, 2017. Uncertain Rule-Based Fuzzy Systems: Introduction and New Directions (2nd Ed.). Springer, Cham, Germany. https://doi.org/10.1007/978-3-319-51370-6

Meng FQ, Tian KS, 2020. Analysis on influence of the bank angle of hypersonic glide vehicle. *J Astronaut*, 41(4):419-428. https://doi.org/10.3873/j.issn.1000-1328.2020.04.005

Miranda SLC, Baker CJ, Woodbridge K, et al., 2007. Fuzzy logic approach for prioritisation of radar tasks and sectors of surveillance in multifunction radar. *IET Radar Sonar Navig*, 1(2):131-141. https://doi.org/10.1049/iet-rsn:20050106

Moreno JE, Sanchez MA, Mendoza O, et al., 2020. Design of an interval type-2 fuzzy model with justifiable uncertainty. *Inform Sci*, 513:206-221. https://doi.org/10.1016/j.ins.2019.10.042

Ontiveros E, Melin P, Castillo O, 2020. Comparative study of interval type-2 and general type-2 fuzzy systems in medical diagnosis. *Inform Sci*, 525:37-53. https://doi.org/10.1016/j.ins.2020.03.059

Ontiveros-Robles E, Melin P, Castillo O, 2018. Comparative analysis of noise robustness of type 2 fuzzy logic controllers. *Kybernetika*, 54(1):175-201. https://doi.org/10.14736/kyb-2018-1-0175

Wang LX, 1999. Analysis and design of hierarchical fuzzy systems. *IEEE Trans Fuzzy Syst*, 7(5):617-624. https://doi.org/10.1109/91.797984

Wu J, Lu F, Zhang JW, et al., 2020. Design of task priority model and algorithm for imaging observation problem. *J Syst Eng Electron*, 31(2):321-334. https://doi.org/10.23919/JSEE.2020.000010

Xiao S, Tan XS, Wang H, et al., 2015. Detection performance assessment of near-space hypersonic target based on ground-based radar. *J Electron Inform Technol*, 37(7):1723-1728 (in Chinese). https://doi.org/10.11999/JEIT141024

Yang SC, Tian KS, Li HQ, et al., 2020. Comprehensive priority-based task scheduling algorithm for anti-missile early warning phased array radar. *Acta Armam*, 41(2):315-323 (in Chinese). https://doi.org/10.3969/j.issn.1000-1093.2020.02.013

Zhang HW, Xie JW, Shi JP, et al., 2017a. Dynamic priority online interleaving scheduling algorithm for the air defense phased array radar. *Syst Eng Electron*, 39(3):529-535 (in Chinese). https://doi.org/10.3969/j.issn.1001-506X.2017.03.11

Zhang HW, Xie JW, Zong BF, et al., 2017b. Dynamic priority scheduling method for the air-defence phased array radar. *IET Radar Sonar Navig*, 11(7):1140-1146. https://doi.org/10.1049/iet-rsn.2016.0549

Zhang HW, Xie JW, Lu WL, et al., 2017c. A scheduling method based on a hybrid genetic particle swarm algorithm for multifunction phased array radar. *Front Inform Technol Electron Eng*, 18(11):1806-1816. https://doi.org/10.1631/FITEE.1601358

Zhang HW, Xie JW, Shi JP, et al., 2018. Online interleaving scheduling algorithm over dynamic priority for the air defense phased array radar. *Acta Electron Sin*, 46(1):55- 60 (in Chinese). https://doi.org/10.3969/j.issn.0372-2112.2018.01.008

Zhang HW, Xie JW, Ge JA, et al., 2019. A hybrid adaptively genetic algorithm for task scheduling problem in the phased array radar. *Eur J Oper Res*, 272(3):868-878. https://doi.org/10.1016/j.ejor.2018.07.012